Goldschmidtite, $(K,REE,Sr)(Nb,Cr)O_3$: a new perovskite supergroup mineral found in diamond from Koffiefontein, South Africa

Nicole A. Meyer*[1], Michelle D. Wenz[2], James P. S. Walsh[3], Steven D. Jacobsen[2], Andrew J. Locock[1], and Jeffrey W. Harris[4]

*corresponding author email: nameyer@ualberta.ca

[1]Department of Earth and Atmospheric Sciences
1-26 Earth Sciences Building
University of Alberta
Edmonton, Alberta, Canada, T6G 2E3

[2]Department of Earth and Planetary Sciences
Northwestern University
2145 Sheridan Road
Technological Institute
Evanston, Illinois, USA, 60208

[3]Department of Chemistry
Northwestern University
2145 Sheridan Road
Evanston, Illinois, USA, 60208

[4]School of Geographical and Earth Sciences
University of Glasgow
The Gregory Building
Lilybank Gardens
Glasgow, Scotland, United Kingdom, G12 8QQ

ABSTRACT

Goldschmidtite is a new perovskite-group mineral (IMA No. 2018-034) with ideal formula (K,REE,Sr)(Nb,Cr)O_3. A single grain of goldschmidtite with maximum dimension of ~100 µm was found as an inclusion in a diamond from the Koffiefontein pipe in South Africa. In addition to the dark green and opaque goldschmidtite, the diamond contained a Cr-rich augite (websteritic paragenesis) and an intergrowth of chromite, Mg-silicate, and unidentified K-Sr-REE-Nb-oxide. Geothermobarometry of the augite indicates the depth of formation was ~170 km. The chemical composition of goldschmidtite determined by electron microprobe analysis (n = 11, WDS, wt%) is: Nb_2O_5 44.82, TiO_2 0.44, ThO_2 0.10, Al_2O_3 0.35, Cr_2O_3 7.07, La_2O_3 11.85, Ce_2O_3 6.18, Fe_2O_3 1.96 MgO 0.70, CaO 0.04, SrO 6.67, BaO 6.82, K_2O 11.53, total 98.53. The empirical formula (expressed to two decimal places) is $(K_{0.50}La_{0.15}Sr_{0.13}Ba_{0.09}Ce_{0.08})_{\Sigma 0.95}(Nb_{0.70}Cr_{0.19}Fe_{0.05}Al_{0.01}Mg_{0.04}Ti_{0.01})_{\Sigma 1.00}O_3$. Goldschmidtite is cubic, space group $Pm\text{-}3m$, with unit-cell parameters: a = 3.9876(1) Å, V = 63.404(6) Å^3, Z = 1, resulting in a calculated density of 5.32(3) g/cm^3. Goldschmidtite is the K-analogue of isolueshite, (Na,La)NbO_3. Raman spectra of goldschmidtite exhibit many second-order broad bands at 100 to 700 cm^{-1} as well as a pronounced peak at 815 cm^{-1}, which is possibly a result of local ordering of Nb and Cr at the B site. The name goldschmidtite is in honor of the eminent geochemist Victor Moritz Goldschmidt (1888 – 1947), who formalized perovskite crystal chemistry and identified $KNbO_3$ as a perovskite-structured compound.

Keywords: perovskite, niobium, mantle, diamond inclusion, new mineral, Koffiefontein, Kaapvaal

INTRODUCTION

Diamonds are carriers of minerals from the lithospheric mantle underpinning cratons (Harris and Gurney 1979; Meyer 1987; Helmstaedt et al. 2010), the mantle transition zone (Pearson et al. 2014; Kiseeva et al. 2015; Tschauner et al. 2018), and the lower mantle (Harte et al. 1999; Tschauner et al. 2014; Palot et al. 2016; Nestola et al. 2018). As a chemically inert and rigid host, diamond can preserve included minerals for billions of years, and thus provide a snapshot of ancient chemical conditions in cratonic keels or deep-mantle regions.

The Kaapvaal craton in South Africa is host to many diamondiferous kimberlites that have been intensively mined and studied since the 1970s (e.g., the International Kimberlite Conferences held since 1973). Large-scale mining, large inclusion-bearing diamonds, and the efforts of geochemists globally, have made the it the most-studied craton from the perspective of diamond formation.

We report the first natural occurrence of (K,REE,Sr)(Nb,Cr)O_3, now named goldschmidtite (IMA No. 2018-034), included in a websteritic diamond from the Koffiefontein kimberlite, Kaapvaal craton, South Africa. The holotype specimen is deposited in the Royal Ontario Museum, accession number M58208. It is the fifth perovskite-structured mineral to occur in Earth's mantle, along with perovskite *sensu stricto* ($CaTiO_3$), bridgmanite (Harte et al. 1999; Tschauner et al. 2014), $CaSiO_3$-perovskite (Nestola et al. 2018), and K-REE-Cr-rich tausonite, which previously recorded the highest Nb- and K-content in a perovskite mineral-inclusion from diamond (Kopylova et al., 1997).

Goldschmidtite is the natural analogue of the well-known ferroelectric material $KNbO_3$, which has the perovskite structure type with orthorhombic symmetry at room temperature (coexisting with a metastable monoclinic phase: Lummen et al. 2017), and whose symmetry increases to cubic above ~400 °C (Skjærvø et al. 2018). Solid solution of $LaFeO_3$ in $KNbO_3$, at molar amounts of 20% or more, also has the effect of increasing the symmetry to cubic at room temperature (Kakimoto et al. 2003).

End-member $KNbO_3$ was first synthesized by Joly (1877), as discussed by Holmquist (1896). Thomas F.W. Barth, a member of Victor Moritz Goldschmidt's research group, was the first to determine the crystal structure of perovskite, $CaTiO_3$ (Barth 1925). In the following year, Goldschmidt and his group reported that $KNbO_3$ was effectively isostructural, and simultaneously introduced the famous tolerance factor for prediction of the perovskite structure type (Goldschmidt 1926).

Goldschmidtite is named in honor of the eminent scientist Victor Moritz Goldschmidt (born Zürich, 27 January 1888; died Oslo, 20 March 1947). Goldschmidt made very wide-reaching contributions in geology, chemistry, mineralogy, crystallography, and petrology (Tilley 1948; Bastiansen 1962; Suess 1988; Mason 1992; Kauffman 1997). He is widely recognized as the "founder of modern geochemistry" (Bastiansen 1962; Kauffman 1997), and as stated by Laves (1962): "The influences of V. M. Goldschmidt's work on the development of mineralogy and crystallography cannot be overestimated."

The name goldschmidtite was briefly used (Hobbs 1899) for a supposed gold-silver telluride, Au_2AgTe_6, that was shown later to be sylvanite (Palache 1900). Similarly, goldschmidtine was used (Peacock 1939) for a supposed antimonide of silver, Ag_2Sb, that was shown subsequently to be stephanite (Peacock 1940). Both of these names had been intended to honor the celebrated crystallographer Victor Mordechai Goldschmidt (born 10 February 10, 1853; died 8 May 1933).

Following the recently revised nomenclature for minerals of the perovskite supergroup (Mitchell et al. 2017), goldschmidtite is a member of the perovskite subgroup and is the potassium-analogue of isolueshite, (Na,La)NbO_3 (Chakhmouradian et al. 1997).

OCCURRENCE

The 90.4 Ma Koffiefontein kimberlite pipe is located about 80 km SSE of Kimberley, South Africa and was emplaced in the Archean basement of the Kaapvaal craton and overlying Phanerozoic sediments of the Karoo basin (Davis 1978; Clement 1982; Naidoo et al. 2004; Field et al. 2008). This diamondiferous kimberlite was discovered in 1870 (Field et al. 2008) and has been mined for diamonds intermittently.

The diamonds from Koffiefontein are dominantly peridotitic (determined from silicate inclusions: Harris and Gurney, 1979; Rickard et al. 1989). Goldschmidtite was found in a websteritic assemblage in association, but not in direct contact, with Cr-rich augite, and an intergrowth of chromite, Mg-silicate, and an unidentified K-Sr-REE-Nb-oxide. In this region of the diamond surface there was both green and brown radiation damage (Figure 1). The Cr-content (1.19 wt% Cr_2O_3) and Mg# (86) of the included augite suggests that the host diamond formed in websterite (Gurney et al. 1984). From single-clinopyroxene geothermobarometry (Nimis and Taylor 2000), an equilibration pressure of 53 kbar (about 170 km depth) and temperature of formation of 1190 °C can be calculated.

EXPERIMENTAL DETAILS

The goldschmidtite inclusion was released from its host diamond by mechanical fracturing of the diamond with a steel diamond cracker. The released mineral was mounted in epoxy, roughly ground with corundum paper, and polished with 1 μm diamond suspension on a nylon cloth.

A Cameca SX100 electron microprobe at the University of Alberta was used to examine a polished and carbon-coated (25 nm thickness) epoxy mount of goldschmidtite. In addition to secondary-electron and back-scattered electron images, quantitative spot analyses were acquired using wavelength-dispersive spectrometry and Probe for EPMA software (Donovan et al. 2015). Nineteen elements were measured (Na, Mg, Al, Si, K, Ca, Ti, Cr, Fe, Sr, Zr, Nb, Ba, La, Ce, Nd, Pr, Sm, and Th) with the following conditions: 20 kV accelerating voltage, 30 nA probe current, and <1 μm beam diameter (5 μm was used for the standards). Total count times of 40 seconds were used for both peaks and backgrounds. The X-ray lines, diffraction crystals, and standards were: Na *K*α, TAP (thallium hydrogen phthalate), albite; Mg *K*α, TAP, pyrope; Al *K*α, TAP, Gore Mountain garnet; Si *K*α, TAP, diopside; K *K*α, PET (pentaerythritol), sanidine; Ca *K*α, PET, diopside; Ti *K*α, PET, $SrTiO_3$; Cr *K*α, LIF, Cr_2O_3; Fe *K*α, LIF (lithium fluoride), fayalite; Sr *L*α, PET, $SrTiO_3$; Zr *L*α, PET, zircon; Nb *L*α, PET, niobium metal; Ba *L*γ, PET, sanbornite; La *L*α, LIF, $LaPO_4$; Ce *L*α, LIF, $CePO_4$; Nd *L*β, LIF, $NdPO_4$; Pr *L*β, LIF, $PrPO_4$; Sm *L*β, LIF, $SmPO_4$; Th *M*α, PET, ThO_2. The X-ray intensity data were reduced following Armstrong (1995) with the mass-absorption coefficients of Chantler et al. (2005). For elements found above the detection limits interference corrections (Donovan et al. 2011) were applied to: Al for interference by Th; Ti for interference by Ba; Cr for interference by La; Fe for interference by Th; Sr for interference by Cr; Ce for interference by Ba; and Th for interference by Cr. The following elements were not found above the limits of detection (as element in weight percent in parentheses): Na (0.01), Si (0.01), Zr (0.04), Pr (0.08), Nd (0.05), and Sm (0.05).

The crystal of goldschmidtite was extracted from the epoxy block and mounted on to a glass fiber with isocyanoacrylate adhesive. High-precision unit-cell parameters were determined by single-crystal X-ray diffraction by the eight-position centering method (King and Finger 1979) on the Huber four-circle diffractometer at Northwestern University equipped with an SMC9300 controller and sealed-tube Mo *K*α radiation source. A 360° phi-rotation image was collected on a MAR345 image plate detector. Full-profile peak fitting was performed with the software package SINGLE (Angel and Finger 2011). In total, 46 reflections were centered using omega scans (rocking curves) in their eight-equivalent positions with a point detector 40 cm from the crystal at 2θ angles between ±30°. Intensity data used to produce a crystallographic information file (.cif) were collected from -15 to +60 degrees 2θ also using the point detector on the four-circle diffraction system at Northwestern University.

Confocal Raman spectroscopy was carried out at Northwestern University using a custom-built system with an Olympus BX microscope with a Mitutoyo 100X objective. A Melles-Griot (Model 85-BLS-601) solid-state, diode-pumped laser with 200 mW output and wavelength of 458.5 nm was used as the excitation source. The output power was reduced with neutral density filters to achieve an ~8 mW focused beam of ~1-2 µm diameter at the sample surface. Unpolarized Raman spectra were collected in back-scatter geometry through a confocal aperture into a 0.5 m focal-length Andor Shamrock 303i spectrograph with 1200 lines-per-mm diffraction grating. Spectra were collected on an Andor Newton DU970 CCD camera cooled to -90 °C with a thermoelectric cooler. Spectra were obtained for 10 seconds, averaged over 12 accumulations for a total of two minutes per spectrum.

RESULTS AND DISCUSSION

Physical and properties

Only a single grain of goldschmidtite, about 100 µm in maximum dimension, was recovered. The mineral is dark green with an adamantine luster, non-fluorescent under longwave UV illumination, and is not cathodoluminescent. The small size of the solitary mineral grain precluded determination of its streak and hardness, and the tenacity, fracture, and cleavage were not observed. From the average chemical composition determined by EPMA and the unit cell parameters, the calculated density is 5.32(3) g/cm^3. The refractive index was calculated to be: n_{calc} 2.16(2), with the use of the Gladstone-Dale constants of Mandarino (1976), the calculated density, and the average chemical composition. Stacked optical images of goldschmidtite acquired with a Tagarno Prestige FHD digital microscope are shown in Figure 2.

Chemical composition

The average composition of goldschmidtite, for elements above detection, is given in Table 1; the iron content is reported as total Fe_2O_3 by analogy with latrappite, $(Ca,Na)(Nb,Ti,Fe)O_3$ (Mitchell et al. 1998). The empirical formula, calculated on the basis of three anions, is: $(K_{0.504}La_{0.150}Sr_{0.133}Ba_{0.092}Ce_{0.078}Ca_{0.002}Th_{0.001})_{\Sigma 0.960}$ $(Nb_{0.695}Cr_{0.192}Fe_{0.051}Al_{0.014}Mg_{0.036}Ti_{0.011})_{\Sigma 0.999}O_3$, which can be simplified to: $(K,REE,Sr)(Nb,Cr)O_3$. The various elements were assigned to the two cation sites (Wyckoff positions 1*b* and 1*a*, respectively) in the aristotypic perovskite formula based on size considerations and following the IMA nomenclature (Mitchell et al. 2017). A back-scattered-electron image of goldschmidtite is shown in Figure 3.

Crystal structure

The method of eight-position centering on a Huber four-circle diffractometer was used to center 46 reflections from ± 30° 2θ, resulting in 368 total rocking curves. The diffraction spots can be described as very sharp, with a full-width at half-maximum averaging 0.07° in the final omega scan. Unconstrained least-squares fitting to all 46 reflections gives unit-cell parameters: a = 3.98757(20) Å, b = 3.98751(22) Å, c = 3.98756(20) Å, α = 89.999(4)°, β = 89.997(4)°, and γ = 89.999(4)°, indicating that goldschmidtite is cubic. Cubic-constrained least squares refinement gives a = 3.98755(12) Å and V = 63.404(6) Å^3.

Single-crystal intensity data were collected in the range of -15 to +60 degrees 2θ, resulting in 753 total reflections in a sphere of reciprocal space from ±5 h, ±5 k and ±5 l, of which 33 are unique with a merging R-factor (R_{int}) of 0.0636. From the intensity data, the space group was determined to be *Pm*-3*m* (No. 221 in the International Tables for Crystallography), being the only space group with zero observed symmetry violations. Although all atoms are on special positions in *Pm*-3*m* (Figure 4), a refinement was carried out to produce anisotropic displacement parameters and a list of reflections and structure factors provided in the crystallographic information file (CIF), yielding a final R-factor of 0.0181. In addition, the powder diffraction pattern was calculated using PowderCell version 2.4 for Windows (Kraus and Nolze 1996) for Cu $K\alpha_1$, 1.540598 Å, and is presented in Table 2. The atom assignments for the powder diffraction calculation were: Wyckoff 1*b* – $(K_{0.504}La_{0.15}Sr_{0.133}Ba_{0.092}Ce_{0.078})_{\Sigma 0.957}$; Wyckoff 1*a* $(Nb_{0.695}Cr_{0.201}Fe_{0.051}Mg_{0.038}Al_{0.014}Ti_{0.011})_{\Sigma 0.999}$; Wyckoff 3*d* – O. Figure 5 shows an unfiltered X-ray diffraction image taken with a MAR345 image plate, demonstrating sharp diffraction spots and the absence of twinning. Goldschmidtite is most similar to isolueshite, $(Na,La,Ca)(Nb,Ti)O_3$

(Krivovichev et al. 2000), which has the identical space group and similar cell dimensions (in the range 3.90-3.91 Å).

Although synthetic $KNbO_3$ is orthorhombic at room temperature, goldschmidtite is cubic. This may be a result of the cation occupancies: the A-site is only 50% filled by K and the B-site is 70% filled by Nb atoms. The balance is filled by smaller-sized cations (e.g., La on the A-site, Cr on the B-site), which results in goldschmidtite adopting a cubic structure as shown for the analogous synthetic system by Kakimoto et al. (2003).

Raman spectrum

Goldschmidtite possesses cubic symmetry, space group *Pm*-3*m*, with A site (K, REE, Sr), B site (Nb, Cr), and O all lying on inversion centers with site symmetry O_h, O_h, and D_{4h}, respectively. Consequently, by selection rules, there are no Raman-active modes. As shown in Figure 6A, the as-measured (uncorrected) Raman spectrum of goldschmidtite exhibits many weak, broad bands from 100-700 cm^{-1} and a large peak at ~815 cm^{-1}, similar to a spectrum of natural perovskite in the RRUFF database (sample R050456) from Magnet Cove, Arkansas, USA, with composition $(Ca_{0.82}Fe_{0.09}Na_{0.07}Ce_{0.01}La_{0.01})(Ti_{0.95}Nb_{0.05})O_3$. In $CaTiO_3$ solid solutions with $Sr(Mg,Nb)O_3$ and $NdAlO_3$, a strong, broad Raman band at ~820 cm^{-1} has been attributed to partial and local ordering of multiple cations on the B site (Zheng et al. 2003; Zheng et al. 2004), suggesting that the 815 cm^{-1} band in goldschmidtite and some $CaTiO_3$ perovskites results from non-random B-site ordering, characteristic of complex perovskites. The broad nature of the 815 cm^{-1} band in goldschmidtite suggests that ordering is short range and weak, which would therefore not be detectable in the single-crystal X-ray diffraction data.

In Figure 6A, the Raman spectrum of goldschmidtite is also compared with natural tausonite from the type locality and synthetic, cubic $SrTiO_3$ from the RRUFF database (sample X090004). Since $SrTiO_3$ also has the *Pm*-3*m* space group, no first-order Raman is expected and the observed bands are second-order features (Schaufele and Weber 1967; Nilsen and Skinner 1968). Second-order Stokes Raman scattering involves the addition or difference combination of phonons from different longitudinal-optical (LO), transverse-optical (TO), or transverse-acoustic (TA) modes (Nilsen and Skinner 1968). In Table 3, the second-order Raman band positions and assignments in $SrTiO_3$ from Nilsen and Skinner (1968) are listed along with the observed bands in goldschmidite from a deconvolution of the baseline-corrected spectrum, shown in Figure 6B. Thus, most of the features in the measured Raman spectrum of goldschmidtite are either attributed to weak, local cation ordering or second-order Raman scattering.

IMPLICATIONS

Potassium and niobium are not common elements in the typical suite of mantle-derived minerals included in diamonds but indicate mantle metasomatism (Erlank and Rickard 1977; Dawson 1982). Several Nb-rich minerals were found in the heavy mineral concentrate from Jagersfontein and from a metasomatic vein in a peridotite from Bultfontein (both kimberlite pipes are in close proximity and age to the Koffiefontein pipe): Nb-rich perovskite (21-28 wt% Nb_2O_5), Nb-rich rutile (~13 wt% Nb_2O_5), Nb-rich titanite (11.9 wt% Nb_2O_5); and were believed form by the interaction of metasomatic fluids with peridotite at 20 to 30 kbar and 900 to 1000 °C (Haggerty et al. 1983). The existence of goldschmidtite indicates that perovskite-structure oxides have the potential to be significant hosts for K and Nb in the mantle, along with other lithophile elements such as La and Ce, and high-field-strength elements such as Ti and Ta. However, the precipitation of a mineral with such high concentrations of LILE (K, Ba) and strongly incompatible HFSE (Sr, LREE, Nb) requires an extremely fractionated metasomatic fluid that is much more enriched in incompatible elements than has been observed for "normal" mantle metasomatism (Hoffman 1988, Allègre et al. 1995). To stabilize such a phase would require that these incompatible elements become major components in the fractionating fluid. Thus, this would likely result from the last drops of an initially much larger volume of metasomatic melt or fluid.

The presence of edgarite, $FeNb_3S_6$, in an unusually reduced fenite (Barkov et al. 2000) has been interpreted recently to indicate that niobium may occur in the trivalent or tetravalent states in the mantle (Bindi and Martin 2018). However, the occurrence of goldschmidtite in diamond suggests that niobium is more likely in the pentavalent state in the mantle, at least in diamond-forming environments.

ACKNOWLEDGEMENTS

The authors thank T. Stachel and D.G. Pearson for their comments and suggestions, which improved the quality of the manuscript. This research was supported in part by the National Research Foundation of South Africa, grant 94626 (N.A. Meyer) and a Natural Sciences and Engineering Research Council (NSERC) Discovery Grant (T. Stachel). S.D. Jacobsen acknowledges support from US National Science Foundation, grant EAR-1853521.

REFERENCES CITED

Allègre, C.J., Poirier, J., Humler, E., and Hofmann, A.W. (1995) The chemical composition of the Earth. Earth and Planetary Science Letters, 134, 515–526.

Angel, R.J. and Finger, L.W. (2011) SINGLE: a program to control single-crystal diffractometers. Journal of Applied Crystallography, 44, 247–251.

Armstrong, J.T. (1995) CITZAF: A package of correction programs for the quantitative electron microbeam X-ray-analysis of thick polished materials, thin-films, and particles. Microbeam Analysis, 4, 177–200.

Barkov, A.Y., Martin, R.F., Men'shikov, Y.P., Savchenko, Y.E., Thibault, Y., and Laajoki, K.V.O. (2000) Edgarite, $FeNb_3S_6$, first natural niobium-rich sulfide from the Khibina alkaline complex, Russian Far North: evidence for chalcophile behavior of Nb in a fenite. Contributions to Mineralogy and Petrology, 138, 229–236.

Barth, T. (1925) Die Kristallstruktur von Perowskit und Verwandten Verbindungen. Norsk Geologisk Tidsskrift, 8, 201–216 (in German).

Bastiansen, O.C.A. (1962) Victor Moritz Goldschmidt 1888–1947. In P.P. Ewald, Ed., Fifty Years of X-Ray Diffraction, pp. 364–365. Springer, Boston, MA.

Bindi, L., and Martin, R.F. (2018) Edgarite, $FeNb_3S_6$, from the Khibina alkaline complex, Russia: solution of the crystal structure. Canadian Mineralogist, 56, 259–264.

Chakhmouradian, A., Yakovenchuk, V., Mitchell, R.H., and Bogdanova, A. (1997) Isolueshite: a new mineral of the perovskite group from the Khibina alkaline complex. European Journal of Mineralogy, 9, 483–490.

Chantler, C.T., Olsen, K., Dragoset, R.A., Chang, J., Kishore, A.R., Kotochigova, S.A. and Zucker, D.S. (2005) X-ray form factor, attenuation and scattering tables, NIST Standard

Reference Database 66 (version 2.1). [Online] Available: http://physics.nist.gov/ffast [2018, August 22]. National Institute of Standards and Technology, Gaithersburg, MD.

Clement, C.R. (1982) A comparative geological study of some major kimberlite pipes in the Northern Cape and Orange Free State. Doctoral dissertation, University of Cape Town.

Davis, G.L. (1978) Zircons from the mantle. Short papers of the Fourth International Conference, Geochronology, Cosmochronology, Isotope Geology. Geological Survey Open-File Report, 78, 86–88.

Dawson, J.B. (1982) Contrasting types of mantle metasomatism. In International Kimberlite Conference: Extended Abstracts, Vol. 3, 232–233.

Donovan, J.J., Kremser, D., Fournelle, J.H., and Goemann, K. (2015) Probe for EPMA: Acquisition, automation and analysis, version 11: Eugene, Oregon, Probe Software, Inc.

Donovan, J.J., Lowers, H.A., and Rusk, B.G. (2011) Improved electron probe microanalysis of trace elements in quartz. American Mineralogist, 96, 274–282.

Erlank, A.J., and Rickard, R.S. (1977) Potassic richterite bearing peridotites from kimberlite and the evidence they provide for upper mantle metasomatism. In International Kimberlite Conference: Extended Abstracts, Vol. 2, 93–95.

Field, M., Stiefenhofer, J., Robey, J., and Kurszlaukis, S. (2008) Kimberlite-hosted diamond deposits of southern Africa: A review. Ore Geology Reviews, 34, 33–75.

Goldschmidt, V.M. (1926) Geochemische Verteilungsgesetze Der Elemente VII. Die Gesetze der Krystallochemie nach Untersuchungen gemeinsam mit T. Barth, G. Lunde, W. Zacharisasen. Skrifter utgitt av det Norske Videnskaps-Akademi i Oslo 1: Matematisk- Naturvidenskapelig Klasse, 1–117 (in German).

Gurney, J.J., Harris, J.W., and Rickard, R.S. (1984) Silicate and oxide inclusions in diamonds from the Orapa Mine, Botswana. In J. Kornprobst, Ed., Kimberlites: II: The Mantle and Crust-Mantle Relationships, 11, p. 3–9. Developments in Petrology, Elsevier, Amsterdam.

Gurney, J.J., Moore, R.O., Otter, M.L., Kirkley, M.B., Hops, J.J., and McCandless, T.E. (1991) Southern African kimberlites and their xenoliths. In: A.B. Kampunza and R.T. Lubala (Eds.), Magmatism in Extensional Structural Settings, pp. 495–536. Springer.

Haggerty, S.E. (1983) The mineral chemistry of new titanates from the Jagersfontein kimberlite, South Africa: implications for metasomatism in the upper mantle. Geochimica et Cosmochimica Acta, 47, 1833–1854.

Harris, J.W., and Gurney, J.J. (1979) Inclusions in Diamond. In J.E. Field, Ed., The Properties of Diamond, pp. 555–591. Academic Press London, London.

Harte, B., Harris, J.W., Hutchison, M.T., Watt, G.R., and Wilding, M.C. (1999). Lower mantle mineral associations in diamonds from Sao Luiz, Brazil. In Y. Fei, C.M. Bertka, and B.O. Mysen, Eds., Mantle Petrology: Field Observations and High-Pressure Experimentation: A Tribute to Francis R. (Joe) Boyd. Geochemical Society Special Publication 6, 125–153.

Helmstaedt, H.H., Gurney, J.J., and Richardson, S.H. (2010) Ages of cratonic diamond and lithosphere evolution: Constraints on Precambrian tectonics and diamond exploration. Canadian Mineralogist, 48, 1385–1408.

Hobbs, W.H. (1899) Goldschmidtite, a new mineral. American Journal of Science, 357–364.

Hofmann, A.W. (1988) Chemical differentiation of the Earth: the relationship between mantle, continental crust, and oceanic crust. Earth and Planetary Science Letters, 90, 297–314.

Holmquist, P.J. (1896) Synthetische Studien über die Perowskit- und Pyrochlormineralien. Bulletin of the Geological Institution of the University of Upsala, 3, 181–268 (in German).

Joly, A. (1877) Recherches sur les composés du niobium et du tantale. Annales Scientifiques de L'École Normal Supérieure, 6, 125–186 (in French).

Kakimoto, K.-I., Masuda, I., and Ohsato, H. (2003) Ferroelectric and piezoelectric properties of $KNbO_3$ ceramics containing small amounts of $LaFeO_3$. Japanese Journal of Applied Physics, 42, 6102–6105.

Kauffman, G.B. (1997) Victor Moritz Goldschmidt (1888–1947): A tribute to the founder of modern geochemistry on the fiftieth anniversary of his death. The Chemical Educator, 2, 1–26.

King, H.E. and Finger, L.W. (1979) Diffracted beam crystal centering and its application to high-pressure crystallography. Journal of Applied Crystallography, 12, 374–378.

Kiseeva, E.S., Wood, B.J., Ghosh, S., and Stachel, T. (2016) The pyroxenite-diamond connection. Geochemical Perspectives Letters, 2, 1–9.

Kopylova, M.G., Gurney, J.J., and Daniels, L.R.M. (1997) Mineral inclusions in diamonds from the River Ranch kimberlite, Zimbabwe. Contributions to Mineralogy and Petrology, 129, 366–384.

Kraus, W., and Nolze, G. (1996) POWDER CELL - a program for the representation and manipulation of crystal structures and calculation of the resulting X-ray powder patterns. Journal of Applied Crystallography, 29, 301–303.

Laves, F. (1962) The growing field of mineral structures. In P.P. Ewald, Ed., Fifty Years of X-Ray Diffraction, pp. 174–189. Springer, Boston, MA.

Lummen, T.T.A., Leung, J., Kumar, A., Wu, X., Ren, Y., VanLeeuwen, B.K., Haislmaier, R.C., Holt, M., Lai, K., Kalinin, S.V., and Gopalan, V. (2017) Emergent low-symmetry phases and large property enhancements in ferroelectric $KNbO_3$ bulk crystals. Advanced Materials, 29, 1700530, 1–7.

Mandarino, J.A. (1976) The Gladstone-Dale relationship - Part I: Derivation of new constants. Canadian Mineralogist, 14, 498–502.

Mason, B.H. (1992) Victor Moritz Goldschmidt: Father of Modern Geochemistry, 184 p. Geochemical Society, Special Publication No. 4, San Antonio.

Meyer, H.O.A. (1987) Inclusions in diamond. In P.H. Nixon, Ed., Mantle Xenoliths, pp. 501–522. John Wiley and Sons.

Mitchell, R.H., Choi, J.B., Hawthorne, F.C., and Burns, P.C. (1998) Latrappite: A re-investigation. Canadian Mineralogist, 36, 107–116.

Mitchell, R.H., Welch, M.D., and Chakhmouradian, A.R. (2017) Nomenclature of the perovskite supergroup: A hierarchical system of classification based on crystal structure and composition. Mineralogical Magazine, 81, 411–461.

Naidoo, P., Stiefenhofer, J., Field, M., and Dobbe, R. (2004) Recent advances in the geology of Koffiefontein Mine, Free State Province, South Africa. Lithos, 76, 161–182.

Nestola, F., Korolev, N., Kopylova, M., Rotiroti, N., Pearson, D.G., Pamato, M.G., Alvaro, M., Peruzzo, L., Gurney, J.J., Moore, A.E., and Davidson, J. (2018) $CaSiO_3$ perovskite in diamond indicates the recycling of oceanic crust into the lower mantle. Nature, 555, 237–241.

Nilsen, W.G., and Skinner, J.G. (1968) Raman spectrum of strontium titanate. Journal of Chemical Physics, 48, 2240–2248.

Nimis, P., and Taylor, W.R. (2000) Single clinopyroxene thermobarometry for garnet peridotites. Part I. Calibration and testing of a Cr-in-Cpx barometer and an enstatite-in-Cpx thermometer. Contributions to Mineralogy and Petrology, 139, 541–554.

Palache, C. (1900) Notes on tellurides from Colorado. American Journal of Science, 419–427.

Palot, M., Jacobsen, S.D., Townsend, J.P., Nestola, F., Marquardt, K., Miyajima, N., Harris, J.W., Stachel, T., McCammon, C.A., and Pearson, D.G. (2016) Evidence for H_2O-bearing fluids in the lower mantle from diamond inclusion. Lithos, 265, 237–243.

Peacock, M.A. (1939) Goldschmidtine, a newly recognized antimonide of silver. American Mineralogist, 24, 227–241.

——— (1940) Goldschmidtine identical with stephanite. American Mineralogist, 25, 372–373.

Pearson, D.G., Brenker, F.E., Nestola, F., McNeill, J., Nasdala, L., Hutchison, M.T., Matveev, S., Mather, K.A., Silversmit, G., Schmitz, S., and others (2014) Hydrous mantle transition zone indicated by ringwoodite included within diamond. Nature, 507, 221–4.

Rickard, R.S., Harris, J.W., Gurney, J.J., and Cardoso, P., (1989) Mineral inclusions in diamonds from Koffiefontein Mine. In Kimberlites and Related Rocks, 2, 1054–1062.

Schaufele, R.F., and Weber, M.J. (1967) First- and second-order Raman scattering of $SrTiO_3$. The Journal of Chemical Physics, 46, 2859–2861.

Skjærvø, S.L., Høydalsvik, K., Blichfeld, A.B., Einarsrud, M.-A., and Grande, T. (2018) Thermal evolution of the crystal structure and phase transitions of $KNbO_3$. Royal Society Open Science, 5, 180368, 1–5.

Suess, H.E. (1988) V.M Goldschmidt and the origin of the elements. Applied Geochemistry, 3, 385–391.

Tilley, C.E. (1948) Victor Moritz Goldschmidt. Biographical Memoirs of Fellows of the Royal Society, 6, 51–66.

Tschauner, O., Ma, C., Beckett, J.R., Prescher, C., Prakapenka, V.B., and Rossman, G.R. (2014) Discovery of bridgmanite, the most abundant mineral in Earth, in a shocked meteorite. Science, 346, 1100–1102.

Tschauner, O., Huang, S., Greenberg, E., Prakapenka, V.B., Ma, C., Rossman, G.R., Shen, A.H., Zhang, D., Newville, M., Lanzirotti, A., and others (2018) Ice-VII inclusions in diamonds: Evidence for aqueous fluid in Earth's deep mantle. Science, 359, 1136–1139.

Zheng, H., Csete de Györgyfalva, G.D.C., Quimby, R., Bagshaw, H., Ubic, R., Reaney, I.M., and Yarwood, J. (2003) Raman spectroscopy of B-site order-disorder in $CaTiO_3$-based microwave ceramics. Journal of the European Ceramic Society, 23, 2653–2659.

Zheng, H., Reaney, I.M., and Gyo, G.D.C.C. De (2004) Raman spectroscopy of $CaTiO_3$-based perovskite.

LIST OF FIGURE CAPTIONS

FIGURE 1. Broken and rounded dodecahedral diamond from Koffiefontein that hosted goldschmidtite (before breakage). Goldschmidtite is seen in green and radiation damage of the diamond can be seen by the brown regions.

FIGURE 2. Two orientations of the crystal of goldschmidtite adhered to a glass fiber. Crystal shape has been affected by polishing. Background noise due to the digital-image stacking has been removed.

FIGURE 3. Back-scattered-electron image of goldschmidtite. The lamellar structure is probably a result of polishing.

FIGURE 4. Clinographic view of the structure of goldschmidtite: Nb atoms are orange and in 6-fold coordination, K is pale blue and in 12-fold coordination, O atoms are red, and the unit cell is shown in black.

FIGURE 5. Unfiltered X-ray diffraction image (Mo *K*α radiation) taken with a MAR345 image plate showing sharp, single diffraction spots and the absence of twinning.

FIGURE 6. **(a)** Uncorrected Raman spectrum of goldschmidtite (black) using a 458.5 nm excitation laser, compared with natural tausonite (red curve) and perovskite (blue curve, RRUFF sample R050456). Spectra are offset for clarity. Raman features in $SrTiO_3$ are attributed to second-order Raman scattering (Nilsen and Skinner 1968). The strong band at 815 cm^{-1} is likely due to weak, local ordering of different cations on the B site (Zheng et al. 2003). **(b)** Deconvolved and baseline-corrected Raman spectrum of goldschmidtite below 1200 cm^{-1}.

TABLE 1. Electron microprobe analysis of goldschmidtite.

Constituent	wt%	Range (n=11)	Stand. dev.
Nb_2O_5	44.82	43.97 – 46.04	0.69
TiO_2	0.44	0.42 – 0.46	0.01
ThO_2	0.1	0 – 0.16	0.06
Al_2O_3	0.35	0.32 – 0.39	0.02
Cr_2O_3	7.07	6.80 – 7.15	0.11
La_2O_3	11.85	11.45 – 12.05	0.17
Ce_2O_3	6.18	6.02 – 6.29	0.08
Fe_2O_3	1.96	1.95 – 1.98	0.01
MgO	0.7	0.67 – 0.78	0.03
CaO	0.04	0.02 – 0.07	0.01
SrO	6.67	6.14 – 6.83	0.21
BaO	6.82	6.48 – 7.30	0.27
K_2O	11.53	11.16 – 11.67	0.14
Total	98.53	97.81 – 99.81	0.58

TABLE 2. Calculated powder diffraction data for goldschmidtite.

Relative intensity, I (%)	$d_{\text{calc.}}$ **(Å)**	***hkl***
0.61	3.9876	100
100.00	2.8197	110
6.89	2.3022	111
49.93	1.9938	200
0.22	1.7833	210
57.80	1.6279	211
35.82	1.4098	220
0.01	1.3292	300
0.05	1.3292	221
28.15	1.2610	310
2.11	1.2023	311
12.89	1.1511	222
0.02	1.1060	320
37.95	1.0657	321
7.30	0.9969	400
0.02	0.9671	410
0.02	0.9671	322
8.63	0.9399	330
17.25	0.9399	411
1.13	0.9148	331
29.88	0.8917	420
0.03	0.8702	421
20.86	0.8502	332
43.24	0.8140	422

TABLE 3. Raman spectral assignments for second-order modes.

Goldschmidtite (cm^{-1})	**$SrTiO_3$ (cm^{-1})[a]**	**Assignments for $SrTiO_3$[a]**
	81	TO_2-TA; TO_2-TO_1
125		
160		
240	251	2TA; $2TO_1$; TO_1+TA
320	308	TO_2+TA; TO_2+TO_1; TO_4-TO_2
	369	TO_4-TA; TO_4-TO_1; $2TO_2$
445		
465		
580		
	629	TO_4+TA; TO_4+TO_1
	684	$2TO_3$
715	727	TO_4+TO_2
750		
815		
850		
	1038	$2LO_2$; $2TO_4$
	1325	LO_4+LO_2
1590	1618	$2LO_4$

[a] Synthetic, pure $SrTiO_3$ (Nilsen and Skinner 1968).

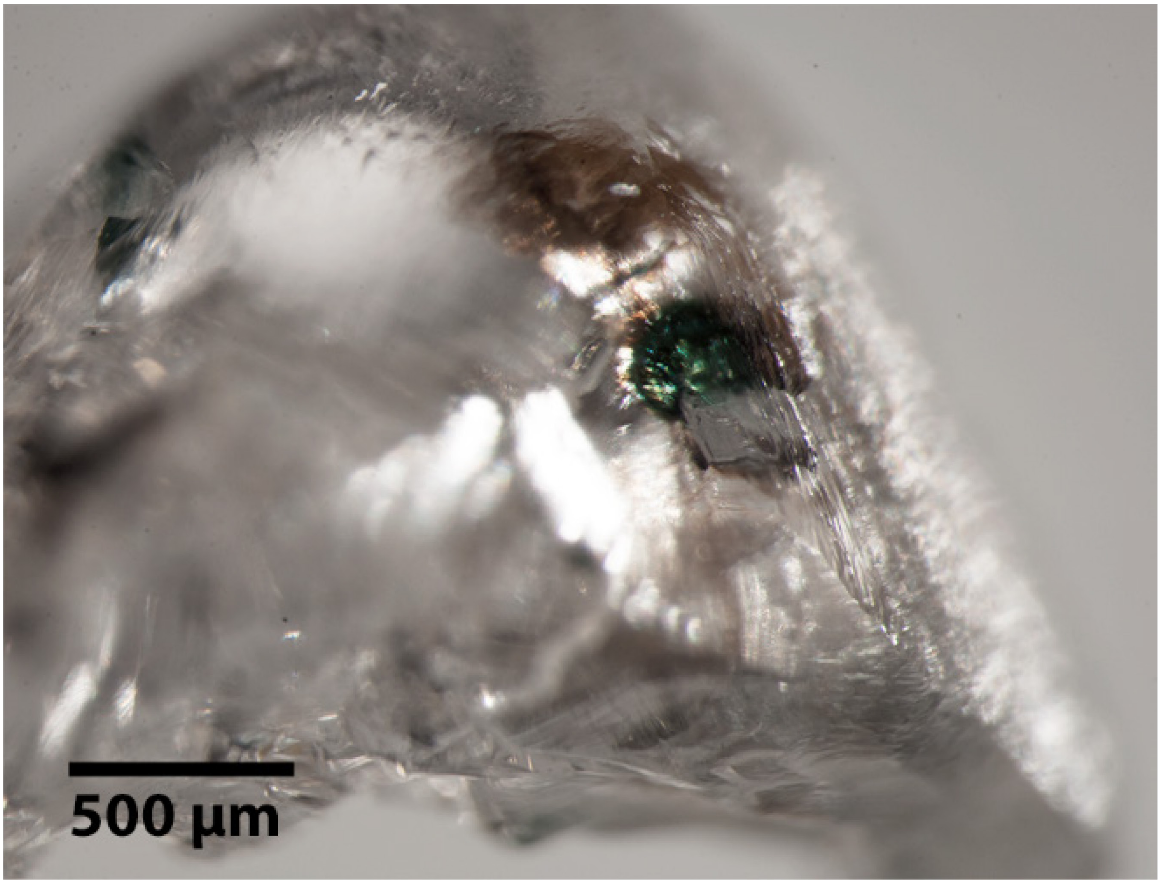

FIGURE 1. Broken and rounded dodecahedral diamond from Koffiefontein that hosted goldschmidtite (before breakage). Goldschmidtite is seen in green and radiation damage of the diamond can be seen by the brown regions.

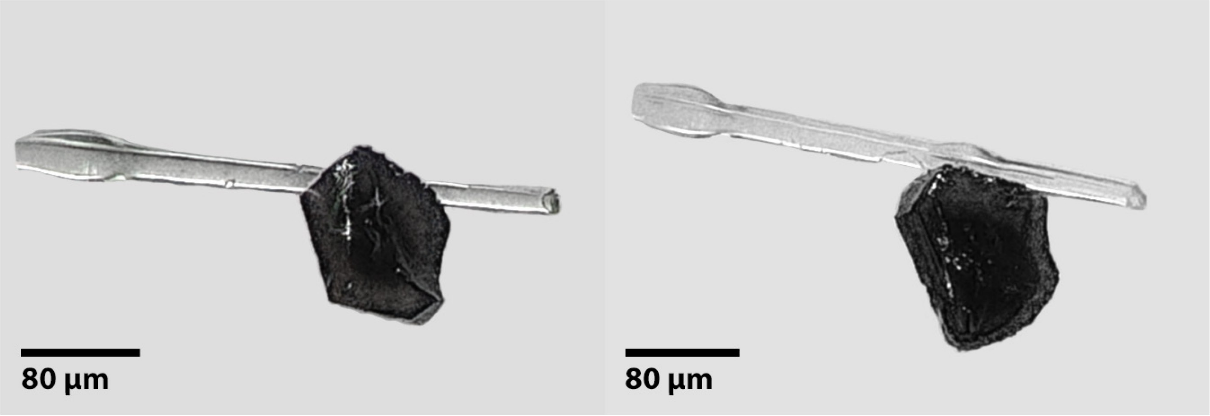

FIGURE 2. Two orientations of the crystal of goldschmidtite adhered to a glass fiber. Crystal shape has been affected by polishing. Background noise due to the digital-image stacking has been removed.

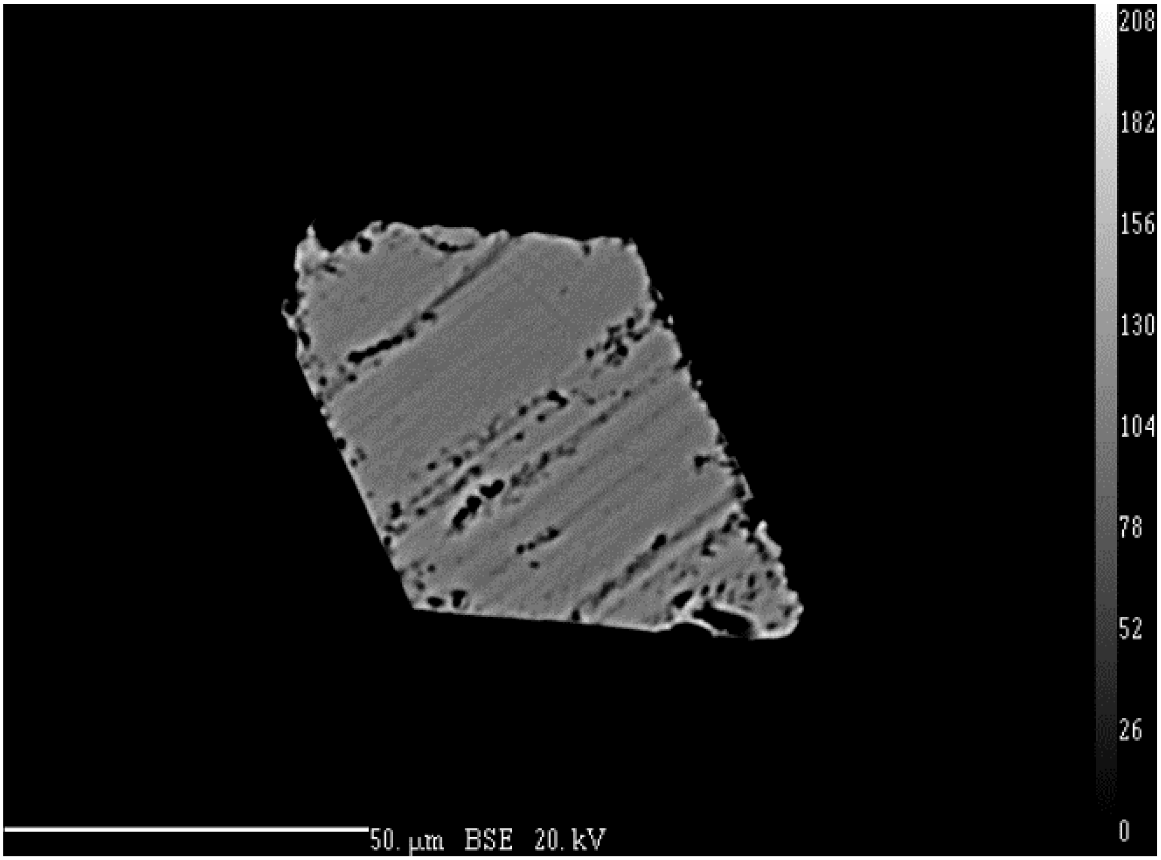

FIGURE 3. Back-scattered-electron image of goldschmidtite. The lamellar structure is probably a result of polishing.

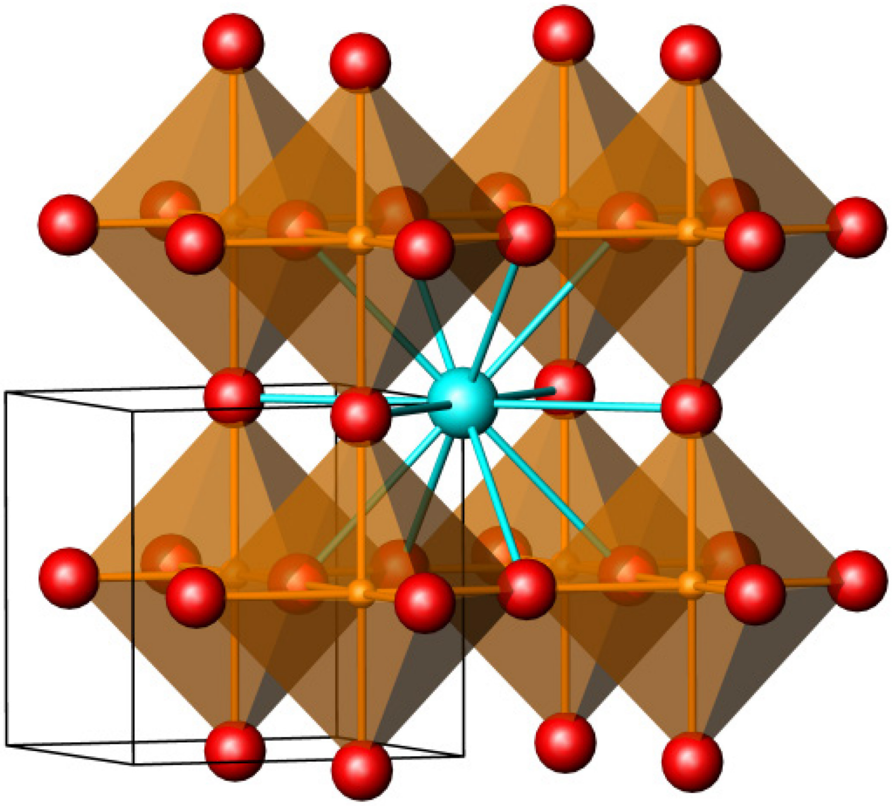

FIGURE 4. Clinographic view of the structure of goldschmidtite: Nb atoms are orange and in 6-fold coordination, K is pale blue and in 12-fold coordination, O atoms are red, and the unit cell is shown in black.

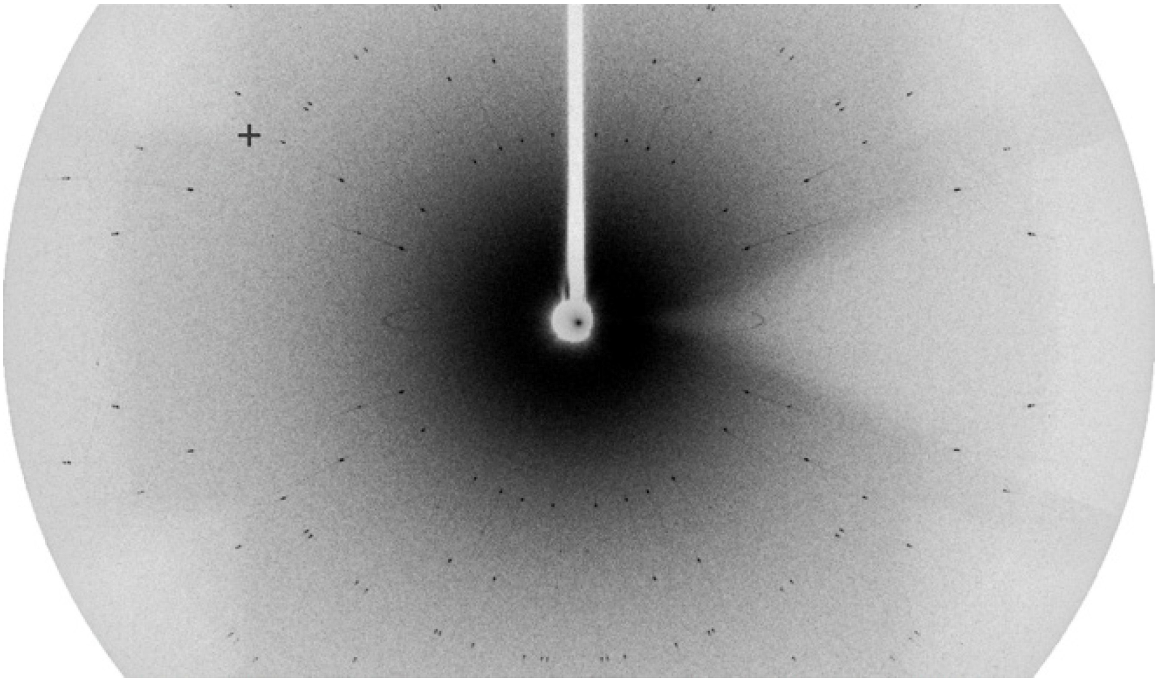

FIGURE 5. Unfiltered X-ray diffraction image (Mo *K*α radiation) taken with a MAR345 image plate showing sharp, single diffraction spots and the absence of twinning.

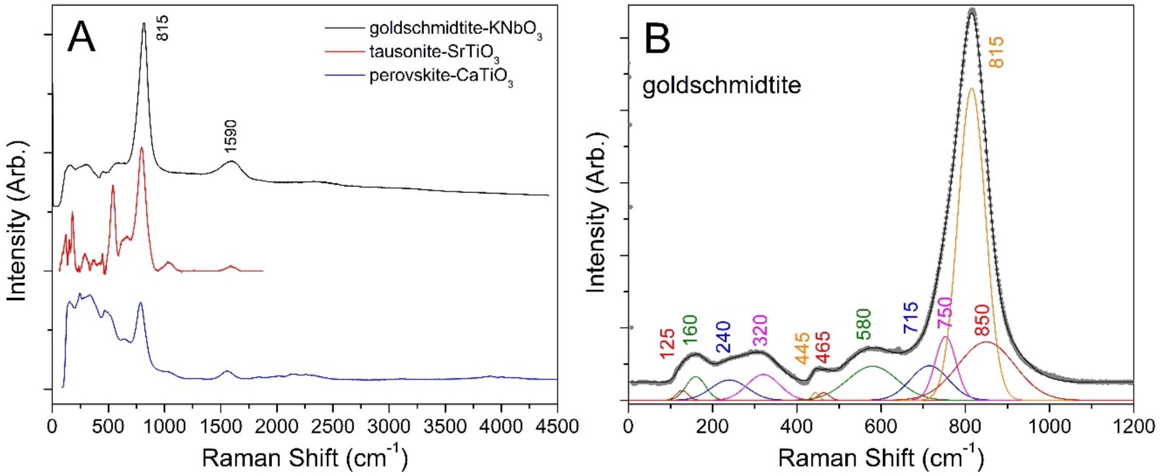

FIGURE 6. (a) Uncorrected Raman spectrum of goldschmidtite (black) using a 458.5 nm excitation laser, compared with natural tausonite (red curve) and perovskite (blue curve, RRUFF sample R050456). Spectra are offset for clarity. Raman features in $SrTiO_3$ are attributed to second-order Raman scattering (Nilsen and Skinner 1968). The strong band at 815 cm^{-1} is likely due to weak, local ordering of different cations on the B site (Zheng et al. 2003). **(b)** Deconvolved and baseline-corrected Raman spectrum of goldschmidtite below 1200 cm^{-1}.